ARTICLES

Journal of Semiconductors
(2024) 45, 032701
doi: 10.1088/1674-4926/45/3/032701

JOS

Behavior of exciton in direct–indirect band gap $Al_xGa_{1-x}As$ crystal lattice quantum wells

Yong Sun[1, 2, †], Wei Zhang[1, 2], Shuang Han[1, 2], Ran An[1, 2], Xin-Sheng Tang[1, 2], Xin-Lei Yu[1, 2], Xiu-Juan Miao[1, 2], Xin-Jun Ma[1, 2, †], Xianglian[1, 2], Pei-Fang Li[1, 2], Cui-Lan Zhao[1, 2], Zhao-Hua Ding[1, 2], and Jing-Lin Xiao[1, 2]

[1]Institute of Condensed Matter Physics, Inner Mongolia Minzu University, Tongliao 028043, China

[2]College of Physics and Electronic Information, Inner Mongolia Minzu University, Tongliao 028043, China

Abstract: Excitons have significant impacts on the properties of semiconductors. They exhibit significantly different properties when a direct semiconductor turns in to an indirect one by doping. Huybrecht variational method is also found to influence the study of exciton ground state energy and ground state binding energy in $Al_xGa_{1-x}As$ semiconductor spherical quantum dots. The $Al_xGa_{1-x}As$ is considered to be a direct semiconductor at Al concentration below 0.45, and an indirect one at the concentration above 0.45. With regards to the former, the ground state binding energy increases and decreases with Al concentration and eigenfrequency, respectively; however, while the ground state energy increases with Al concentration, it is marginally influenced by eigenfrequency. On the other hand, considering the latter, while the ground state binding energy increases with Al concentration, it decreases with eigenfrequency; nevertheless, the ground state energy increases both with Al concentration and eigenfrequency. Hence, for the better practical performance of the semiconductors, the properties of the excitons are suggested to vary by adjusting Al concentration and eigenfrequency

Key words: exciton effects; aluminum gallium arsenide crystal; direct band gap semiconductor; indirect band gap semiconductor

Citation: Y Sun, W Zhang, S Han, R An, X S Tang, X L Yu, X J Miao, X J Ma, Xianglian, P F Li, C L Zhao, Z H Ding, and J L Xiao, Behavior of exciton in direct–indirect band gap $Al_xGa_{1-x}As$ crystal lattice quantum wells[J]. *J. Semicond.*, 2024, 45(3), 032701. https://doi.org/10.1088/1674-4926/45/3/032701

1. Introduction

Numerous experimental and theoretical research works have been conducted in recent years on semiconductor quantum well, quantum well lines and quantum dots[1–4]. Moreover, the limitation of carrier motion in all three spatial dimensions is considered to be an essential property of quantum dots. Special property can be widely used in technological applications[5–7]. Furthermore, the reduction in the size of a quantum dot is demonstrated to lead to partial or complete quantization of energy levels, which ameliorate the physical properties of these systems. Hence, various quasi-particles in quantum dots have been the focus of numerous researchers[8–11].

The state of the exciton in semiconductors have been shown to play a key role in the absorption and luminescence spectra understanding the basic photoelectric properties of artificial layered materials[12–16]. Accordingly, exciton properties in semiconductor quantum devices have become an important topic of research in condensed matter physics. Moreover, studies on the state of exciton in quantum dots have mainly considered the confinement effect of potential well, such as the finite barrier potential[17, 18], valence-band mixing[19], dispersion relation[20, 21], mass[22–24], dielectric constant mismatch[25, 26], etc. Qualitative and quantitative results obtained from exciton binding energy and energy level are consistent with the experimental results[27–29]. In addition, adopting the effective phonon approximation method, the exciton-phonon interaction has been extensively investigated[30–32]. This is while the linear combination operator method has been rarely utilized in studying excitons in quantum dots. Hence, using the linear combination operator method, the present study aims at investigating the effect of exciton in the $Al_xGa_{1-x}As$ crystals.

In addition, Huybrecht variational method was used in the present research to study the ground state energy and ground state binding energy of exciton in quantum dots in $Al_xGa_{1-x}As$ crystals. Numerical simulation was also applied to study the relationship between exciton energy level and binding energy with eigenfrequency and Al concentration. Hence, with regards to low-dimensional semiconductor materials, the obtained results are expected to have important theoretical significance.

2. Theoretical model

As can be seen in Fig. 1(a), aluminum gallium arsenide is an atomic semiconductor material formed by doping Al atoms into GaAs. In the above formula, x is a number ranging from 0 to 1, which shows an arbitrary alloy between Ga and Al atoms in $Al_xGa_{1-x}As$. Moreover, due to the different electronegativity and atomic size of Al and Ga atoms in $Al_xGa_{1-x}As$ crystal, short range potential is generated in the lattice and, accordingly, bound exciton is formed. The exciton Hamiltonian in this system is formulated as:

Correspondence to: Y Sun, sy19851009@126.com; X J Ma, maxiaoguang80@126.com

Received 2 SEPTEMBER 2023; Revised 6 NOVEMBER 2023.

©2024 Chinese Institute of Electronics

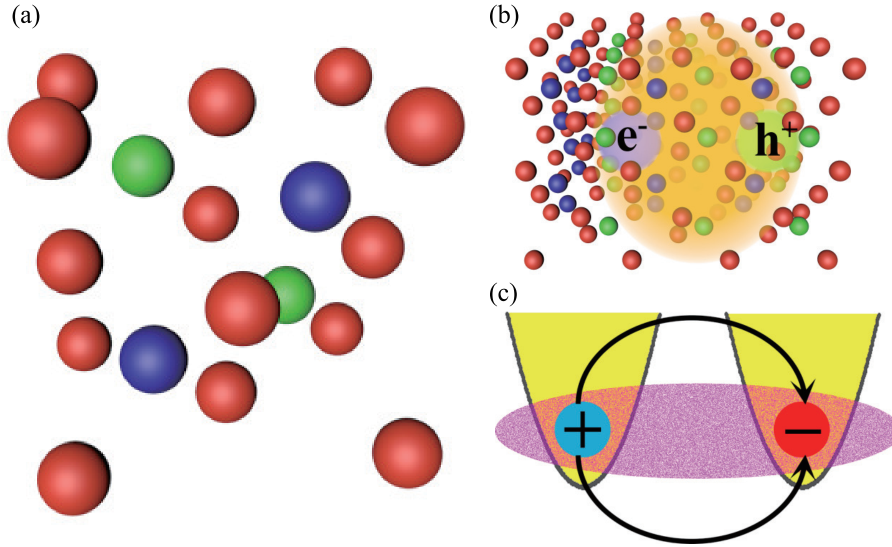

Fig. 1. (Color online) (a) Schematic diagram of $Al_xGa_{1-x}As$ ground state lattice; (b) schematic diagram of exciton–phonon coupling in $Al_xGa_{1-x}As$ crystals; (c) schematic diagram of an exciton subject to parabolic potential.

$$H=-\frac{\hbar^2}{2\mu_e}\nabla_e^2-\frac{\hbar^2}{2\mu_h}\nabla_h^2-\frac{e^2}{\varepsilon_\infty|\mathbf{r}_e-\mathbf{r}_h|}+\sum_{\mathbf{W}}\hbar\omega_{LO}a_{\mathbf{W}}^{\dagger}a_{\mathbf{W}}+\sum_{\mathbf{W}}[V_W a_{\mathbf{W}}(\exp(i\mathbf{W}\cdot\mathbf{r}_h)-\exp(i\mathbf{W}\cdot\mathbf{r}_e))+h.c]+U(\mathbf{r}_e)+U(\mathbf{r}_h), \tag{1}$$

$$U(r_{e,h})=\frac{1}{2}\mu_{e,h}\omega_0^2\mathbf{r}_{e,h}^2. \tag{2}$$

While first and the second terms on the right-hand side of Eq. (1) are electron and hole movements, respectively, the third term describes the Coulomb potential between electron–hole interaction. Moreover, the fourth and the fifth terms define the phonon energy and the interaction energy of exciton–phonon coupling, (Fig. 1(b)), respectively. Furthermore, while the parabolic potentials of electrons is expressed by the sixth term, holes are described by the seventh term (Fig. 1(c)). In addition, V_W and α can be written as:

$$V_W=\frac{4ei\pi}{\sqrt{V}}\left(\frac{c\hbar\omega_{LO}}{8\pi W^2}\right)^{1/2}, c=\frac{1}{\varepsilon_\infty}-\frac{1}{\varepsilon_0}, \tag{3}$$

$$\alpha=\frac{Me^2}{\hbar^2u}\left(\frac{1}{\varepsilon_\infty}-\frac{1}{\varepsilon_0}\right), \tag{4}$$

$$\frac{\hbar^2u^2}{2M}=\hbar\omega_{LO}. \tag{5}$$

Here $\varepsilon_\infty(\varepsilon_0)$ denotes the high frequency (static) permittivity of the material.

In order to transform the Hamiltonian into a Hamiltonian in centroid coordinates, the following definition is provided:

$$M=\mu_e+\mu_h, \mathbf{R}=\beta_e\mathbf{r}_e+\beta_h\mathbf{r}_h=\frac{\mu_e}{M}\mathbf{r}_e+\frac{\mu_h}{M}\mathbf{r}_h, \tag{6}$$

$$\mu=\frac{\mu_e\mu_h}{\mu_e+\mu_h}, \mathbf{r}=\mathbf{r}_e-\mathbf{r}_h, \tag{7}$$

$$\beta_e=\frac{\mu_e}{M}, \beta_h=\frac{\mu_h}{M}, \tag{8}$$

$$\xi_{\mathbf{W}}=\left(e^{-i\beta_e\mathbf{W}\cdot\mathbf{r}}-e^{i\beta_h\mathbf{W}\cdot\mathbf{r}}\right). \tag{9}$$

Here M denotes the total mass of exciton, $\mathbf{R}$ represents the coordinate of the center-of-mass describing the motion of the center of mass, μ stands for the reduced mass, and $\mathbf{r}$ signifies the relative coordinate relating to the internal relative motion of exciton. Accordingly, the Hamiltonian at center-of-mass coordinates can be formulated as:

$$H^*=-\frac{\hbar^2}{2M}\nabla_R^2-\frac{\hbar^2}{2\mu}\nabla_r^2-\frac{e^2}{\varepsilon_\infty r}+\sum_{\mathbf{W}}\hbar\omega_{LO}a_{\mathbf{W}}^{\dagger}a_{\mathbf{W}}+\sum_{\mathbf{W}}[V_W a_{\mathbf{W}}\exp(i\mathbf{W}\cdot\mathbf{R})\xi_{\mathbf{W}}+h.c]+\frac{1}{2}M\omega_0^2\mathbf{R}^2+\frac{1}{2}\mu\omega_0^2r^2. \tag{10}$$

Subsequently, the following two unitary transformations[33] are performed for Eq. (10).

$$U_1=\exp\left(-i\sum_{\mathbf{W}}\mathbf{W}\cdot\mathbf{R}a_{\mathbf{W}}^{\dagger}a_{\mathbf{W}}\right), \tag{11}$$

$$U_2=\exp\left(\sum_{\mathbf{W}}a_{\mathbf{W}}^{\dagger}f_W-a_{\mathbf{W}}f_W^*\right). \tag{12}$$

Here $f_W(f_W^*)$ represents the variational parameters of unitary transformation. Meanwhile, the following relations introduce the linear combination operators of the creation (annihilation) operator $B_j^{\dagger}(B_j)$ of the electron and variational parameter λ[34]

$$\mathbf{P}_j=\left[\frac{M\hbar\lambda}{2}\right]^{\frac{1}{2}}\left(B_j+B_j^{\dagger}\right), \tag{13}$$

$$\mathbf{R}_j=i\left[\frac{\hbar}{2M\lambda}\right]^{\frac{1}{2}}\left(B_j-B_j^{\dagger}\right). \tag{14}$$

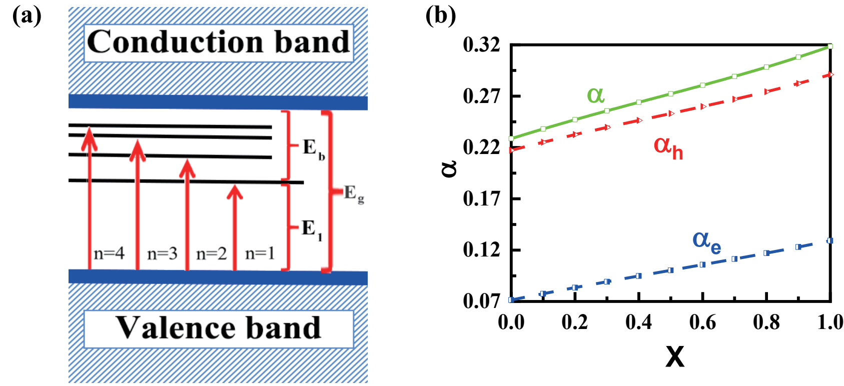

Fig. 2. (Color online) (a) Schematic diagram of exciton energy band. (b) Relationship between exciton and phonon coupling coefficient and Al concentration.

$$j = x, y, z. \tag{15}$$

The transformed Hamiltonian of the system can be expressed as:

$$\begin{aligned} H = {} & \frac{\hbar\lambda\left(B_j B_j + 2B_j^{\dagger} B_j + B_j^{\dagger} B_j^{\dagger}\right)}{4} + \frac{3\hbar\lambda}{4} - \frac{-2\sum_{\mathbf{W}} \hbar \mathbf{W}\left(a_{\mathbf{W}}^{\dagger} + f_W^{*}\right)\left(a_{\mathbf{W}} + f_W\right)\left[\frac{M\hbar\lambda}{2}\right]^{\frac{1}{2}}\left(B_j + B_j^{\dagger}\right)}{2M} + \\ & \frac{\sum_{\mathbf{W}} \hbar^2 W^2\left(a_{\mathbf{W}}^{\dagger} + f_W^{*}\right)\left(a_{\mathbf{W}} + f_W\right)}{2M} + \frac{\sum_{\mathbf{W}} \hbar^2 W^2\left(a_{\mathbf{W}}^{\dagger} + f_W^{*}\right)\left(a_{\mathbf{W}}^{\dagger} + f_W^{*}\right)\left(a_{\mathbf{W}} + f_W\right)\left(a_{\mathbf{W}} + f_W\right)}{2M} - \\ & \frac{\hbar^2}{2\mu}\frac{\partial^2}{\partial r^2} - \frac{\hbar^2}{\mu}\left(\sum_{\mathbf{W}} a_{\mathbf{W}}^{\dagger}\nabla f_W - a_{\mathbf{W}}\nabla f_W^{*}\right)\nabla\varphi - \varphi\frac{\hbar^2}{2\mu}\left(\sum_{\mathbf{W}} a_{\mathbf{W}}^{\dagger}\nabla^2 f_W - a_{\mathbf{W}}\nabla^2 f_W^{*}\right) - \\ & \frac{1}{2!}\frac{\hbar^2}{\mu}\sum_{\mathbf{W}}\left(a_{\mathbf{W}}^{\dagger}a_{\mathbf{W}}^{\dagger}\nabla f_W\nabla f_W - 2a_{\mathbf{W}}^{\dagger}a_{\mathbf{W}}\nabla f_W^{*}\nabla f_W - \nabla f_W\nabla f_W^{*} + a_{\mathbf{W}}a_{\mathbf{W}}\nabla f_W^{*}\nabla f_W^{*}\right) + \\ & \frac{e^2}{\varepsilon_\infty r} + \sum_{\mathbf{W}}\hbar\omega_{\mathrm{LO}}\left(a_{\mathbf{W}}^{\dagger} + f_W^{*}\right)\left(a_{\mathbf{W}} + f_W\right) + \sum_{\mathbf{W}}\left[V_W\left(a_{\mathbf{W}} + f_W\right)\xi_{\mathbf{W}} + h.c\right] - \\ & \frac{\omega_0^2\hbar}{4\lambda}\sum_j\left(B_j^2 + B_j^{\dagger 2} - 2B_j^{\dagger}B_j - \delta_{jj}\right) + \frac{1}{2}\mu\omega_0^2 r^2. \end{aligned} \tag{16}$$

Now, let us assume that the ground state normalized wave function $\psi = \varphi(r)\left|0\right\rangle$ is chosen, where $\left|0\right\rangle$ satisfies $B_j\left|0\right\rangle = a_{\mathbf{W}}\left|0\right\rangle = 0$. $\varphi(r)$ is wave function describing the relative motion of the system. Due to the influence of the parabolic potential, $\varphi(r)$ can be written as:

$$\left|\varphi(r)\right\rangle = (\pi)^{-\frac{3}{4}}\lambda_0^{\frac{3}{2}}\exp\left(\frac{-\lambda_0^2 r^2}{2}\right). \tag{17}$$

Here, the expectation value of the total energy can be described as:

$$\begin{aligned} E(\lambda,\lambda_0,r) = \left\langle\varphi(r)\right| H \left|\varphi(r)\right\rangle = {} & \frac{3\hbar^2\lambda_0^2}{4m} - \frac{2e^2\lambda_0}{\sqrt{\pi}\varepsilon_\infty} + \frac{3}{4}\hbar\lambda + 2\alpha\hbar\omega_{\mathrm{LO}}\left[-1 + \mathrm{Exp}\left[\frac{u^2}{4\lambda_0^2}\right]\mathrm{Ercf}\left[\frac{u}{2\lambda_0}\right]\right] + \\ & \alpha\hbar\omega_{\mathrm{LO}}\frac{M}{\mu}\left[\frac{1}{2}\left(\beta_{\mathrm{e}}^2 + \beta_{\mathrm{h}}^2\right) + \beta_{\mathrm{e}}\beta_{\mathrm{h}}\left[\frac{-2u + \dfrac{\mathrm{Exp}\left[\frac{u^2}{4\lambda_0^2}\right]\sqrt{\pi}\left(2\lambda_0^2 + u^2\right)\mathrm{Erfc}\left[\frac{u}{2\lambda_0}\right]}{\lambda_0}}{2\lambda_0\sqrt{\pi}}\right]\right] + \frac{3\omega_0^2\hbar}{4\lambda} + \frac{3\mu\omega_0^2}{4\lambda_0^2}. \end{aligned} \tag{18}$$

Here $\mathrm{Erfc}\left[\frac{u}{2\lambda_0}\right] \approx 0$ as $\frac{u}{2\lambda_0} \gg 2$. Thus, $F(\lambda,\lambda_0,r)$ variational is made to λ, λ_0, i.e $\frac{\partial E(\lambda,\lambda_0,r)}{\partial\lambda} = 0$, $\frac{\partial E(\lambda,\lambda_0,r)}{\partial\lambda_0} = 0$. Accordingly, we can obtain:

$$\frac{3}{4}\hbar - \frac{3\omega_0^2\hbar}{4\lambda^2} = 0, \tag{19}$$

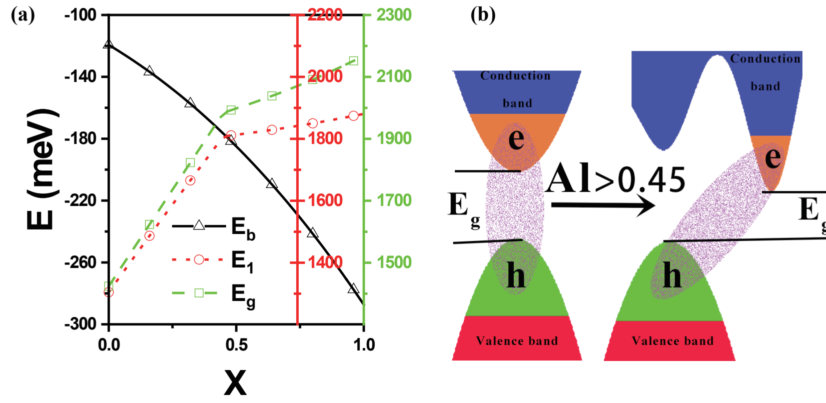

Fig. 3. (Color online) Exciton energy in $Al_xGa_{1-x}As$ crystal: (a) At $\omega_0 = 10^{13}$ Hz, E_b, E_1 and E_g change with Al concentration in $Al_xGa_{1-x}As$ crystal; (b) schematic diagram of exciton energies in direct semiconductors and indirect semiconductors.

$$\frac{3\hbar^2\lambda_0}{2\mu} - \frac{2e^2}{\sqrt{\pi}\varepsilon_\infty} + \frac{\alpha\beta_e\beta_h\hbar M\omega_{LO}}{\mu\lambda_0^2\sqrt{\pi}} - \frac{3\mu\omega_0^2}{2\lambda_0^3} = 0. \tag{20}$$

The ground state binding energy of the exciton (Fig. 2(a)) is obtained by bringing λ, λ_0 back to $F(\lambda, \lambda_0, r)$:

$$E_b = \frac{3\hbar^2\lambda_0^2}{4m} - \frac{2e^2\lambda_0}{\sqrt{\pi}\varepsilon_\infty} + \frac{3}{4}\hbar\lambda - 2\alpha\hbar\omega_{LO} + \alpha\hbar\omega_{LO}\frac{M}{\mu}\left[\frac{1}{2}\left(\beta_e^2+\beta_h^2\right) - \frac{u\beta_e\beta_h}{\sqrt{\pi}\lambda_0}\right] + \frac{3\omega_0^2\hbar}{4\lambda} + \frac{3\mu\omega_0^2}{4\lambda_0^2}. \tag{21}$$

The exciton ground state energy (Fig. 2(a)) is:

$$E_0 = E_g + \frac{3\hbar^2\lambda_0^2}{4m} - \frac{2e^2\lambda_0}{\sqrt{\pi}\varepsilon_\infty} + \frac{3}{4}\hbar\lambda - 2\alpha\hbar\omega_{LO} + \alpha\hbar\omega_{LO}\frac{M}{\mu}\left[\frac{1}{2}\left(\beta_e^2+\beta_h^2\right) - \frac{u\beta_e\beta_h}{\sqrt{\pi}\lambda_0}\right] + \frac{3\omega_0^2\hbar}{4\lambda} + \frac{3\mu\omega_0^2}{4\lambda_0^2}. \tag{22}$$

3. Discussion

The numerical results obtained from the analytical research of selecting $Al_xGa_{1-x}As$ crystal are discussed. In the following, the exciton parameters in the $Al_xGa_{1-x}As$ crystal[35–37] are shown in Table 1.

Table 1. Related parameters of $Al_xGa_{1-x}As$ crystals.

	GaAs	$Al_xGa_{1-x}As$	AlAs
m_e (units of m_0)	0.067	$0.067 + 0.083x$	0.15
m_h (units of m_0)	0.62	$0.62 + 0.14x$	0.76
$\hbar\omega_{LO}$ (meV)	36.25	$36.25 + 38.3x + 17.12x^2 - 5.11x^3$	50.09
ε_0	13.18	$13.18 - 3.12x$	10.06
ε_∞	10.89	$10.89 - 2.73x$	8.16
E_g (eV)	1.424	$1.424 + 1.247x, x < 0.45$ $1.9 + 0.125x + 0.143x^2, x > 0.45$	2.168

Despite that all the exciton energies E_b, E_1 and E_g increased with an increase in the Al concentration of $Al_xGa_{1-x}As$ crystals, certain differences were observed. As can be seen in Fig. 3(a), GaAs and AlAs are direct and indirect semiconductors, respectively. Moreover, an increase in the Al concentration leads the $Al_xGa_{1-x}As$ crystal to change from a direct to an indirect semiconductor when $x > 0.45$ (Fig. 3(b)). Furthermore, the comparison of the bandgap energy E_g when $x < 0.45$ with the bandgap energy E_g when $x > 0.45$, revealed a rapid increase in the bandgap energy E_g when $Al_xGa_{1-x}As$ is a direct semiconductor; this is while the rate of the increase was found to slow down when $Al_xGa_{1-x}As$ is an indirect semiconductor. Furthermore, an increase in the Al concentration was observed to uniformly increase the exciton ground state binding energy E_b, which did not vary by the properties of semiconductor. In addition, the exciton ground state energy E_1 was found to rapidly increase when $x < 0.45$, but remains almost unchange when $x > 0.45$. In the following, the underlying reasons for this phenomenon are discussed and investigated.

As can be seen in Figs. 4(a) and 4(b), an increase in the Al component was found to lead to an increase in the ground state binding energy and ground state energy of exciton. However, the opposite trend was observed for the ground state energy and the ground state binding energy of exciton. This is to say that while an increase in the eigenfrequency led to a decrease in the ground state binding energy of the exciton, it resulted in an increase in the ground state energy. More importantly, while varying material properties did not change the ground state binding energy, this was not the case for the ground state energy. The ground state binding energy represents the energy that binds electrons and holes together. As can be seen in Fig. 2(b), coupling between the exciton and phonon is enhanced with with an increase in Al concentration. This, accordingly, enhances the exciton self-trapping effect, which in turn inhibits the ability of the exciton to pass through the crystal and raises the binding energy. As can be seen in Figs. 4(c) and 4(d), by an increase in the eigenfrequency, more electrons and holes are bound to their respective positions, which accordingly, causes the exciton to be more stable and more difficult to recombine. This, in turn, leads to an increase and a decrease in the binding energy and the ground state energy, respectively. Using a simple approximation method, Chuu *et al.*[36] studied the subband structure and the binding energy of an exciton in the GaAs/AlGaAs superlattice. Both the exciton binding energy and the subband energy were expressed as a function of well width, barrier width, and Al composition. They also considered the influence of the effective-mass mismatch. The

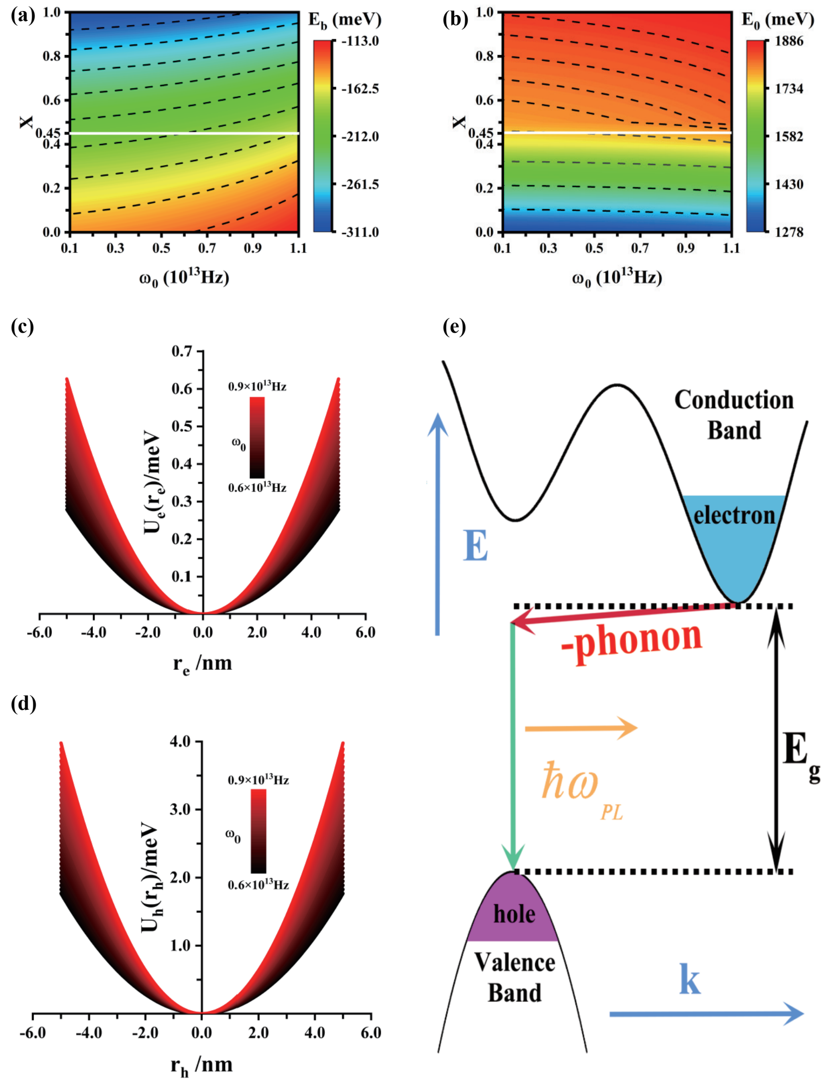

Fig. 4. (Color online) (a) The influence of quantum dots and Al concentration on exciton ground state binding energy; (b) the dependence of exciton ground state binding energy on quantum dots and Al concentration; (c) the parabolic potential of the electron; (d) the parabolic potential of the hole; (e) schematic diagram of an exciton in an indirect semiconductor.

energy spacings between the interband or the intersubband transitions were calculated and compared with the observed data, which revealed a good agreement. While the width of the bandgap is considered to be the main difference between the direct and the indirect semiconductors, the ground state binding energy is almost unaffected by this factor. In other words, the binding energy is unaffected by variation in the properties of the material. Furthermore, since the ground state energy of an exciton determines the energy of the exciton recombination, variation in the bandgap is expected to directly affect the ground state energy. Also, in case of a direct semiconductor, an increase in the Al concentration leads to the enhancement of the exciton self-trapping effect. Consequently, the ability of the exciton to pass through the crystal is inhibited. So, the exciton is limited to a smaller range, resulting in the reduction of the energy required for the exciton recombination. Moreover, electrons and holes are located in the conduction and the valence bands, respectively. Therefore, an increase in the eigenfrequency causes them to be more strongly restricted in the conduction and the valence bands (see Figs. 4(c) and 4(d)), resulting in more stable exciton. However, during the exciton recombination process (see Fig. 4(e)), the presence of phonon extinction results in a minimal effect of exciton-phonon interaction on the exciton state. Additionally, the exciton recombination is accompanied with a change in electron-hole momentum, which leads to a weak effect of the confined intensity.

4. Conclusion

Applying the linear combination operator and unitary transformation methods, the present study investigated the ground state binding energy and ground state energy of exciton in $Al_xGa_{1-x}As$ semiconductor. The isotropic parabolic potential and the Al concentration were also studied. Accordingly, the following results are drawn:

(1) The bandgap energy of $Al_xGa_{1-x}As$ semiconductor was observed to change by an increase in Al concentration. Moreover, while the $Al_xGa_{1-x}As$ semiconductor was found to be a direct semiconductor at Al concentration below 0.45, the $Al_xGa_{1-x}As$ semiconductor was observed to be an indirect one at Al concentration above 0.45;

(2) While the ground state binding energy of the exciton was found to always increase with an increase in the Al concentration, it decreased with an increase in the eigenfre-

quency and, accordingly, not influenced by variations in the properties of the semiconductor;

(3) When the $Al_xGa_{1-x}As$ semiconductor was direct, the ground state energy of exciton increased with the increase of Al concentration; however, in the case where the semiconductor was indirect, slight changes were observed in the ground state energy of exciton with an increase in the Al concentration. Hence, the obtained results and properties can significantly contribute to the experimental studies on correlation exciton effect.

Moreover, the findings of the study can potentially be used in adjusting the exciton energy level in band gap engineering of semiconductor doping as well as for studying the luminescent properties of materials.

Acknowledgment

The project is supported by the National Natural Science Foundation of China (Nos. 12164032 and 11964026), the Natural Science Foundation of Inner Mongolia (No. 2019MS01010), Scientific Research Projects in Colleges and Universities in Inner Mongolia (No. NJZZ19145), Graduate Science Innovative Research Projects (No. S20210281Z), the Natural Science Foundation of Inner Mongolia (No. 2022MS01014), Doctor Research Start-up Fund of Inner Mongolia Minzu University (No. BS625).

References

[1] Dong H L, Jia T T, Liang J, et al. Improved carrier transport and photoelectric properties of InGaN/GaN multiple quantum wells with wider well and narrower barrier. Opt Laser Technol, 2020, 129, 106309

[2] Liu N, Hu G W, Dan M J, et al. Piezo-phototronic effect on quantum well terahertz photodetector for continuously modulating wavelength. Nano Energy, 2019, 65, 104091

[3] Xia L P, Huang J N, Zhou E, et al. A photoelectric synapse based on optimized perovskite $CH_3NH_3PbBr_3$ quantum dot film detectors. Appl Phys Lett, 2022, 120, 261112

[4] Liu Y, Du L Y, Gu K K, et al. Effect of Tm dopant on luminescence, photoelectric properties and electronic structure of In_2S_3 quantum dots. J Lumin, 2020, 217, 116775

[5] Wang X, Feng Y Q, Dong P P, et al. A mini review on carbon quantum dots: Preparation, properties, and electrocatalytic application. Front Chem, 2019, 7, 671]

[6] Liu F, Ding C, Zhang Y H, et al. GeI_2 additive for high optoelectronic quality $CsPbI_3$ quantum dots and their application in photovoltaic devices. Chem Mater, 2019, 31, 798

[7] Gong X, Guan L, Li Q W, et al. Black phosphorus quantum dots in inorganic perovskite thin films for efficient photovoltaic application. Sci Adv, 2020, 6, eaay5661

[8] Lorenz S, Erickson C S, Riesner M, et al. Directed exciton magnetic polaron formation in a single colloidal Mn^{2+}: CdSe/CdS quantum dot. Nano Lett, 2020, 20, 1896

[9] Ma X J, Zhang W, Han S A, et al. The level-splitting effects of spin-orbit interaction on strong-coupling polaron in quantum dots with alkali halide. Phys E, 2022, 144, 115387

[10] Deng Y Z, Lin X, Fang W, et al. Deciphering exciton-generation processes in quantum-dot electroluminescence. Nat Commun, 2020, 11, 2309

[11] Fobasso M F C, Fotue A J, Kenfack S C, et al. Stability and coherence of strong-coupling magneto-bipolaron in asymmetric quantum dot under laser field effect. Phys Lett A, 2018, 382, 3490

[12] Konishi K, Naka N. Phonon-assisted excitonic absorption in diamond. Phys Rev B, 2021, 104, 125204

[13] Geiregat P, Rodá C, Tanghe I, et al. Localization-limited exciton oscillator strength in colloidal CdSe nanoplatelets revealed by the optically induced stark effect. Light, 2021, 10, 112

[14] Qin M B, Duan J Y, Xiao S Y, et al. Manipulating strong coupling between exciton and quasibound states in the continuum resonance. Phys Rev B, 2022, 105, 195425

[15] Gao X, Shen Y Q, Liu J J, et al. Boosting the photon absorption, exciton dissociation, and photocatalytic hydrogen- and oxygen-evolution reactions by built-in electric fields in Janus platinum dichalcogenides. J Mater Chem C, 2021, 9, 15026

[16] Morozov S, Wolff C, Mortensen N A. Room-temperature low-voltage control of excitonic emission in transition metal dichalcogenide monolayers. Adv Opt Mater, 2021, 9, 2101305

[17] Alijabbari M, Mehramiz A, Mafi A. The energy states of an electron in a spheroidal quantum dot with finite barrier. Superlattices Microstruct, 2019, 133, 106180

[18] Hbibi M, Mommadi O, Chouef S, et al. Finite confinement potentials, core and shell size effects on excitonic and electron-atom properties in cylindrical core/shell/shell quantum dots. Sci Rep, 2022, 12, 14854

[19] Ji B T, Rabani E, Efros A L, et al. Dielectric confinement and excitonic effects in two-dimensional nanoplatelets. ACS Nano, 2020, 14, 8257

[20] Klahold W M, Choyke W J, Devaty R P. Band structure properties, phonons, and exciton fine structure in 4H-SiC measured by wavelength-modulated absorption and low-temperature photoluminescence. Phys Rev B, 2020, 102, 205203

[21] Qiu D Y, Cohen G, Novichkova D, et al. Signatures of dimensionality and symmetry in exciton band structure: Consequences for exciton dynamics and transport. Nano Lett, 2021, 21, 7644

[22] Baranowski M, Plochocka P, Su R, et al. Exciton binding energy and effective mass of $CsPbCl_3$: A magneto-optical study: Publisher's note. Photon Res, 2022, 10, 2447

[23] Liu Y, Wang J, Zhu N, et al. Investigation on binding energy and reduced effective mass of exciton in organic–inorganic hybrid lead perovskite films by a pure optical method. Opt Lett, 2019, 44, 3474

[24] Jahanshir A. Relativistic modification of the exciton's mass in monolayer TMDCs materials. Journal of Advanced Materials and Processing, 2020, 8(4), 45

[25] Chafai A, Essaoudi I, Ainane A, et al. Nonlinear optical characteristics of an exciton in a GaSb-capped InSb heterodot: Role of size control. Eur Phys J Plus, 2020, 135, 203

[26] Chen X H, Lu H P, Wang K, et al. Tuning spin-polarized lifetime in two-dimensional metal–halide perovskite through exciton binding energy. J Am Chem Soc, 2021, 143, 19438

[27] Zheng R S, Matsuura M. Exciton binding energies in polar quantum wells with finite potential barriers. Phys Rev B, 1998, 58, 10769

[28] Filinov A V, Riva C, Peeters F M, et al. Influence of well-width fluctuations on the binding energy of excitons, charged excitons, and biexcitons in GaAs-based quantum wells. Phys Rev B, 2004, 70, 035323

[29] Baranowski M, Plochocka P. Excitons in metal-halide perovskites. Adv Energy Mater, 2020, 10, 1903659

[30] Adamska L, Umari P. Bethe-Salpeter equation approach with electron-phonon coupling for exciton binding energies. Phys Rev B, 2021, 103, 075201

[31] Huang T A, Zacharias M, Lewis D K, et al. Exciton–phonon interactions in monolayer germanium selenide from first principles. J Phys Chem Lett, 2021, 12, 3802

[32] Shree S, Semina M, Robert C, et al. Observation of exciton-phonon coupling in $MoSe_2$ monolayers. Phys Rev B, 2018, 98, 035302

[33] Lee T D, Low F E, Pines D. The motion of slow electrons in a polar crystal. Phys Rev, 1953, 90, 297

[34] Huybrechts W J. Internal excited state of the optical polaron. J Phys C, 1977, 10, 3761
[35] Hai G Q, Peeters F M, Devreese J T. Polaron energy and effective mass in a quantum well. Phys Rev B, 1990, 42, 11063
[36] Chuu D S, Lou Y C. Exciton binding energy and subband structures of GaAs/$Al_xGa_{1-x}As$ superlattices. Phys Rev B, 1991, 43, 14504
[37] Liu W. Fundamentals of III-V devices: HBTs, MESFETs, and HFETs/HEMTs. Wiley, 1999

Yong Sun received his doctoral degree form Tianjin University, Tianjin, China, in 2021. He is currently an Associate professor withthe College of Physics and Electronic Information, Inner Mongolia Minzu University, Tongliao, China. His current research interests include direct-indirect band gap III-V compound semiconductor materials.

Xin-Jun Ma received his doctoral degree form Jilin University, Changchun, China, in 2018. He is currently a professor with the College of Physics and Electronic Information, Inner Mongolia Minzu University, Tongliao, China. His research interests include low dimensional materials.